Supplement of The Cryosphere, 18, 957–976, 2024
https://doi.org/10.5194/tc-18-957-2024-supplement

The Cryosphere
Open Access

Supplement of

Effects of Arctic sea-ice concentration on turbulent surface fluxes in four atmospheric reanalyses

Tereza Uhlíková et al.

Correspondence to: Tereza Uhlíková (tereza.uhlikova@helsinki.fi)

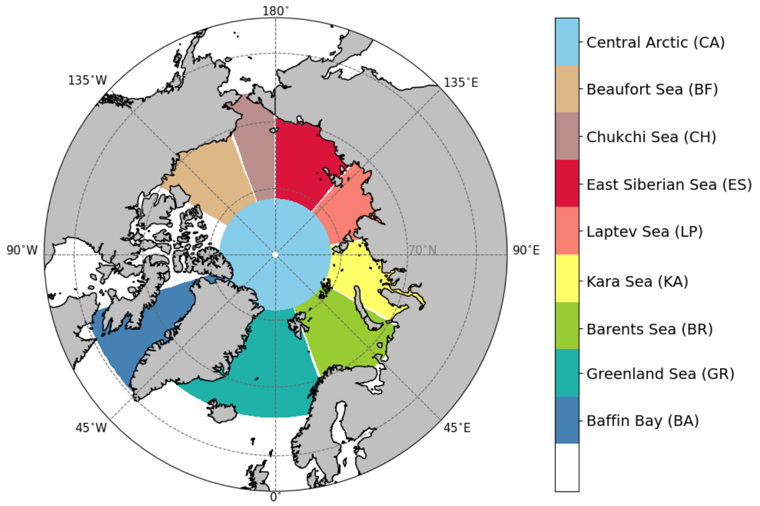

Figure S 1: Arctic basins used for calculating daily field means of sensible heat flux in Table S1 and Figure S2.

Table S 1: Mean sensible heat flux (W m^{-2}) in Arctic basins as parameterised in NCEP/CFSR in November–December–January (NDJ), February–March–April (FMA), May–June–July (MJJ), and August–September–October (ASO); in time periods 1980–2000 (I) and 2001–2021 (II).

Season	**NDJ**		**FMA**		**MJJ**		**ASO**	
Time period	I	II	I	II	I	II	I	II
Central Arctic	11	15	13	14	4	2	4	7
Beaufort Sea	11	12	10	11	5	4	1	1
Chukchi Sea	1	-1	9	11	6	5	-5	-4
East Siberian Sea	13	12	10	11	6	5	3	2
Laptev Sea	6	5	5	5	3	3	1	0
Kara Sea	0	-6	3	0	3	2	-2	-3
Barents Sea	-49	-41	-33	-37	-1	-1	-12	-8
Greenland Sea	-40	-31	-35	-32	-2	-2	-9	-7
Baffin Bay	-19	-19	-14	-13	1	2	-3	-2

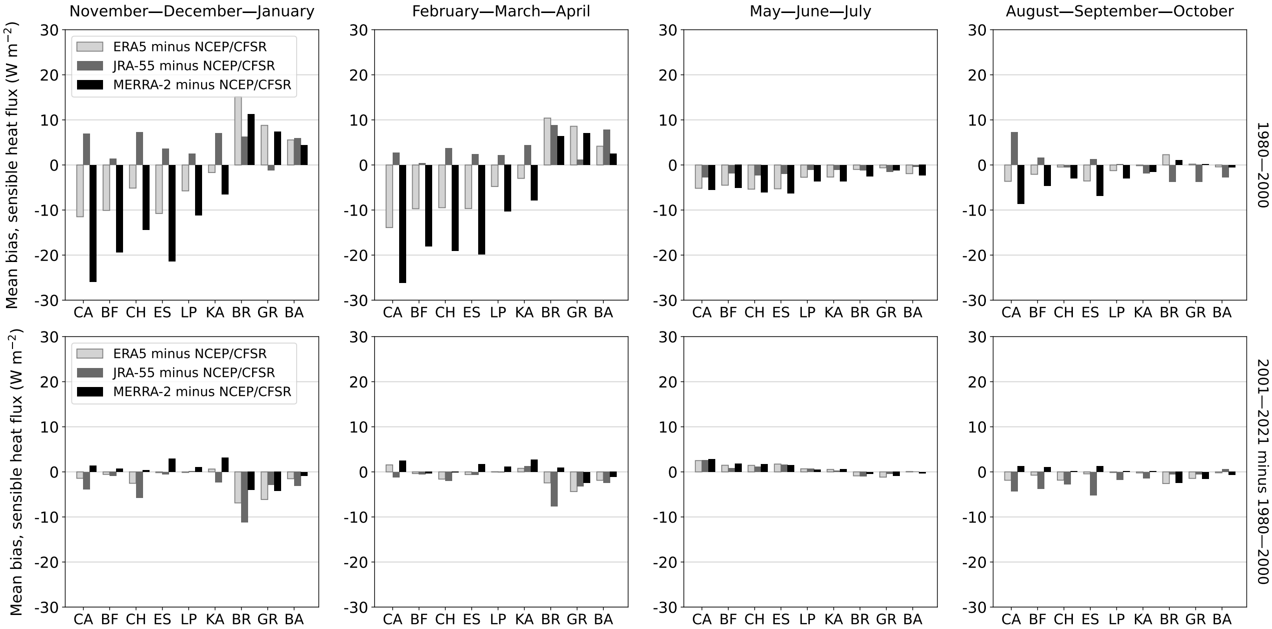

Figure S 2: Mean Biases of Daily Field Means of sensible heat flux: ERA5 minus NCEP/CFSR (light grey), JRA-55 minus NCEP/CFSR (grey), and MERRA-2 minus NCEP/CFSR (black). Horizontal axis refers to Arctic basins as seen in Figure S1. The first row shows data from period 1980–2000 and the second row the 2001–2021 difference from the earlier period. Only grid cells fully covered by the sea were considered in this analysis.

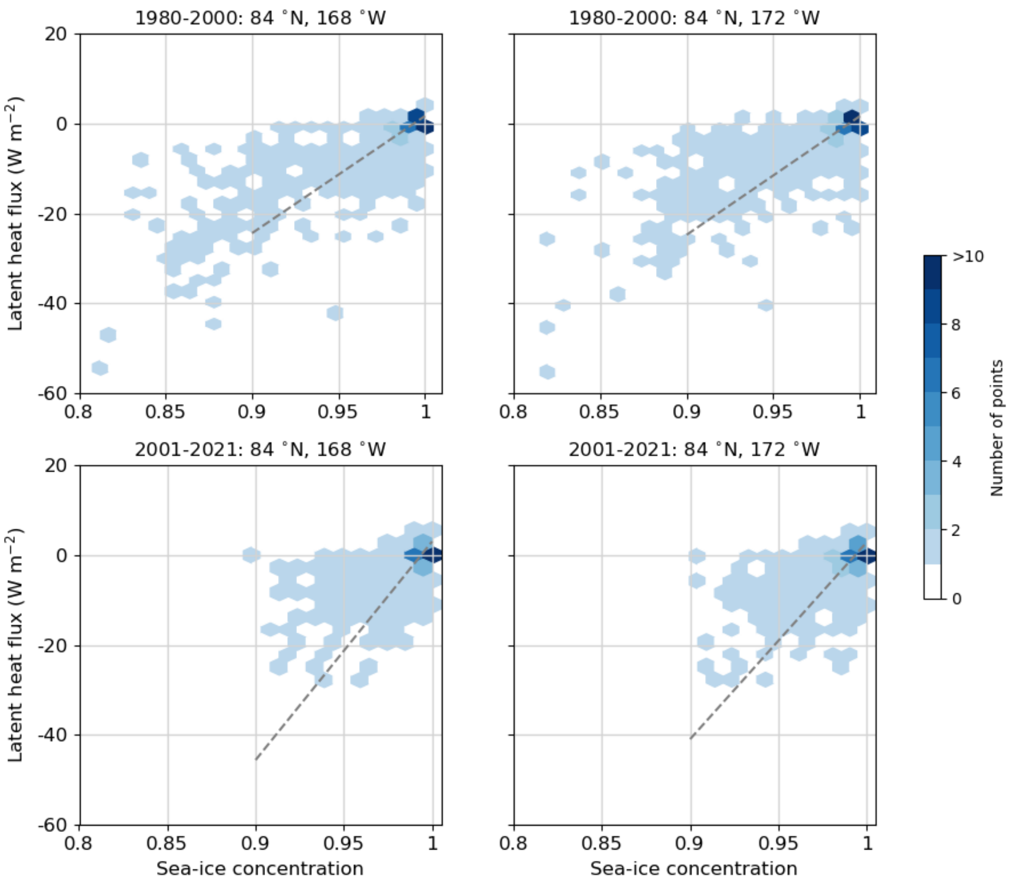

Figure S 3: Daily sea-ice concentration and latent heat flux in two selected grid cells from the Central Arctic (columns, nearest to 84° N, 168° W and nearest to 84° N, 172° W), where the sensitivity of latent heat flux to sea-ice concentration increased between 1980–2000 and 2001–2021; NCEP/CFSR data, November–December–January. Orthogonal-distance-regression lines are indicated by dashed grey lines (steeper in 2001–2021).

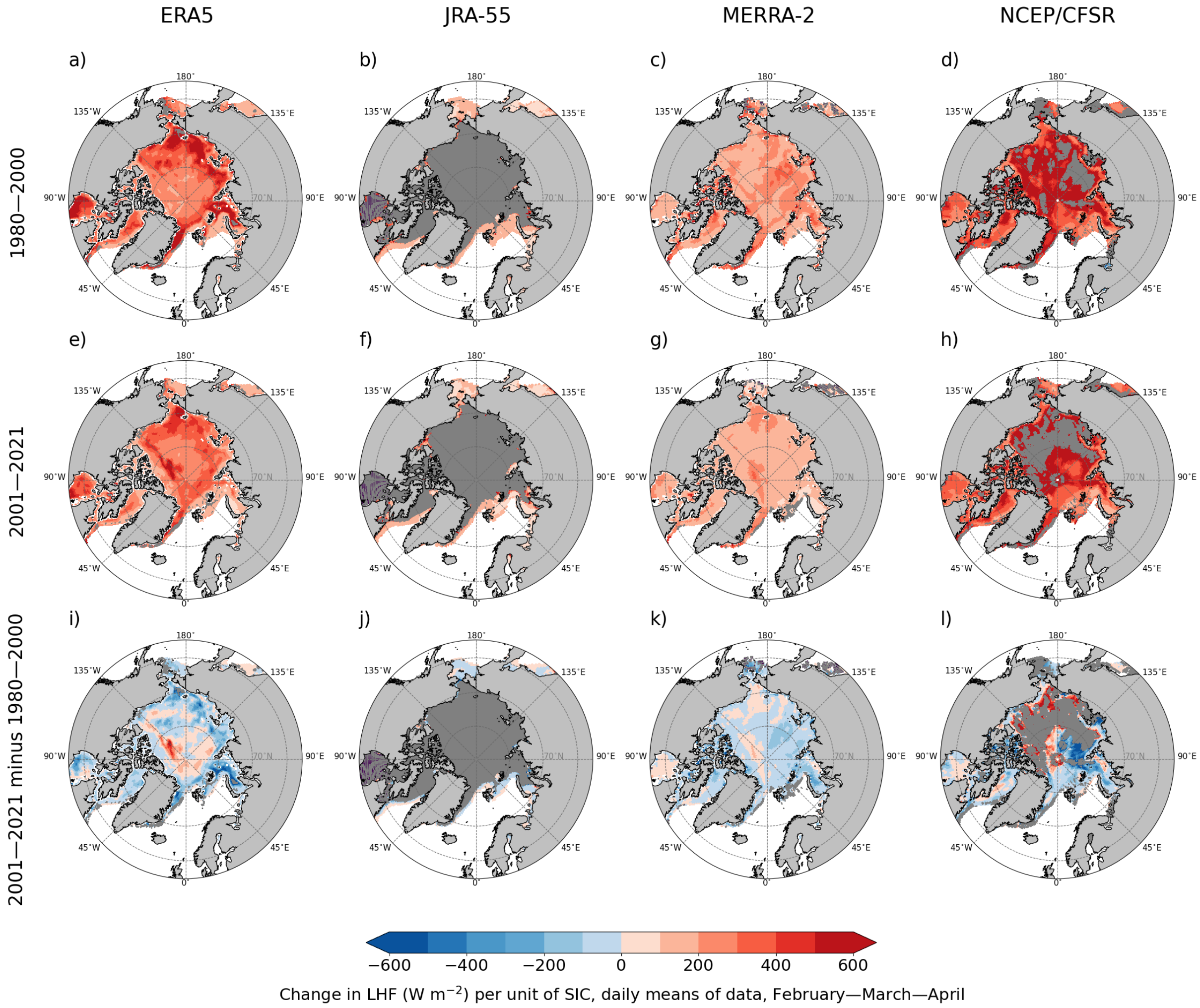

Figure S 4: Change in latent heat flux (W m^{-2}) per unit of change in sea-ice concentration (slope of regression line) in four reanalyses (columns), marine Arctic, February–March–April, based on the linear orthogonal-distance-regression (ODR) model. **a–d** depict the period 1980–2000, **e–h** period 2001–2021, and **i–l** show the 2001–2021 difference from 1980–2000. Dark grey indicates areas where the ODR model did not converge; in i–l, dark grey shows these areas in 1980–2000 and/or 2001–2021. Only grid cells with a mean of SIC > 0.5 were considered, and only statistically significant results within 95 % confidence interval are shown.

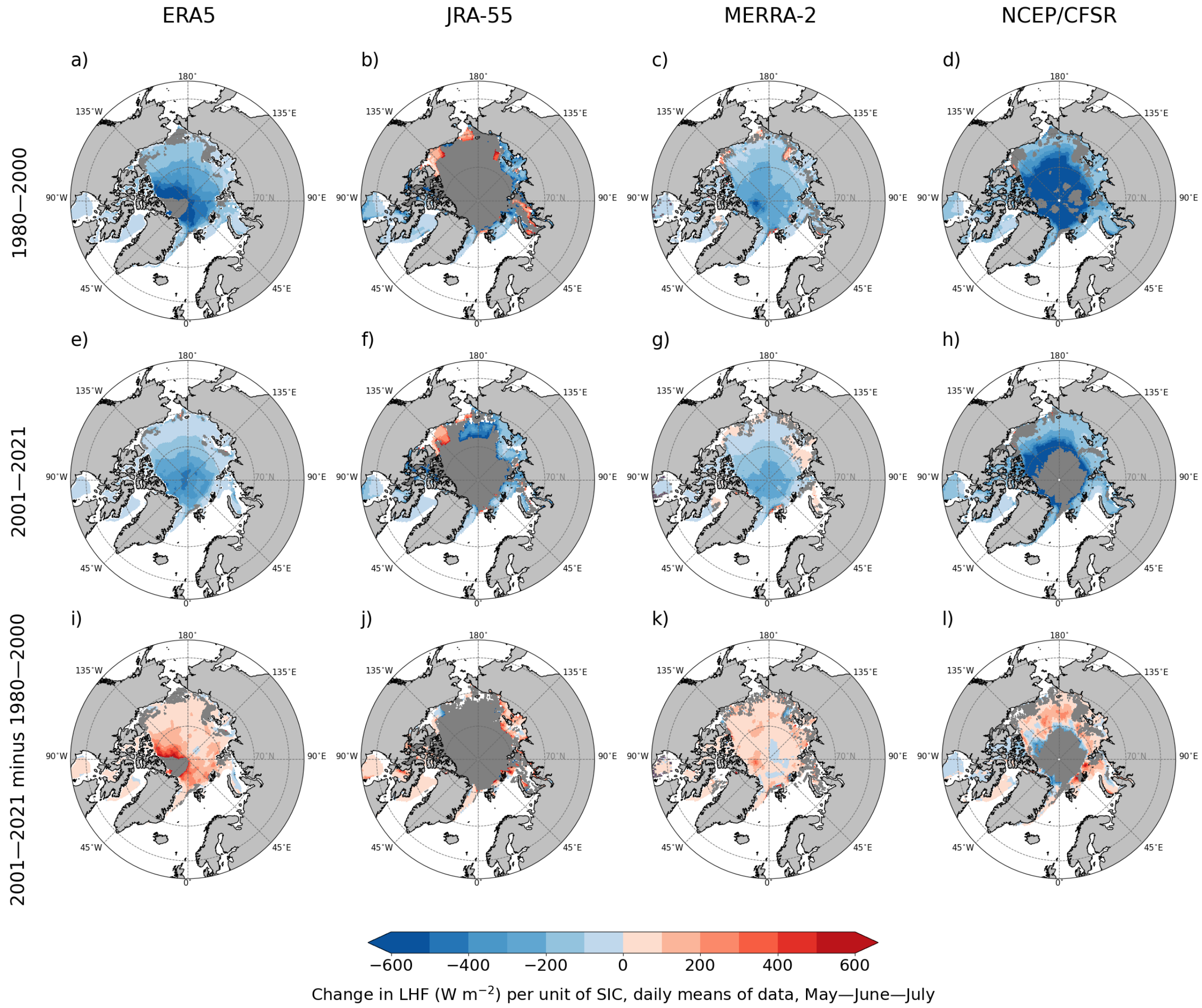

Figure S 5: Change in latent heat flux (W m^{-2}) per unit of change in sea-ice concentration (slope of regression line) in four reanalyses (columns), marine Arctic, May–June–July, based on the linear orthogonal-distance-regression (ODR) model. **a**–**d** depict the period 1980–2000, **e**–**h** period 2001–2021, and **i**–**l** show the 2001–2021 difference from 1980–2000. Dark grey indicates areas where the ODR model did not converge; in i–l, dark grey shows these areas in 1980–2000 and/or 2001–2021. Only grid cells with a mean of SIC > 0.5 were considered, and only statistically significant results within 95 % confidence interval are shown.

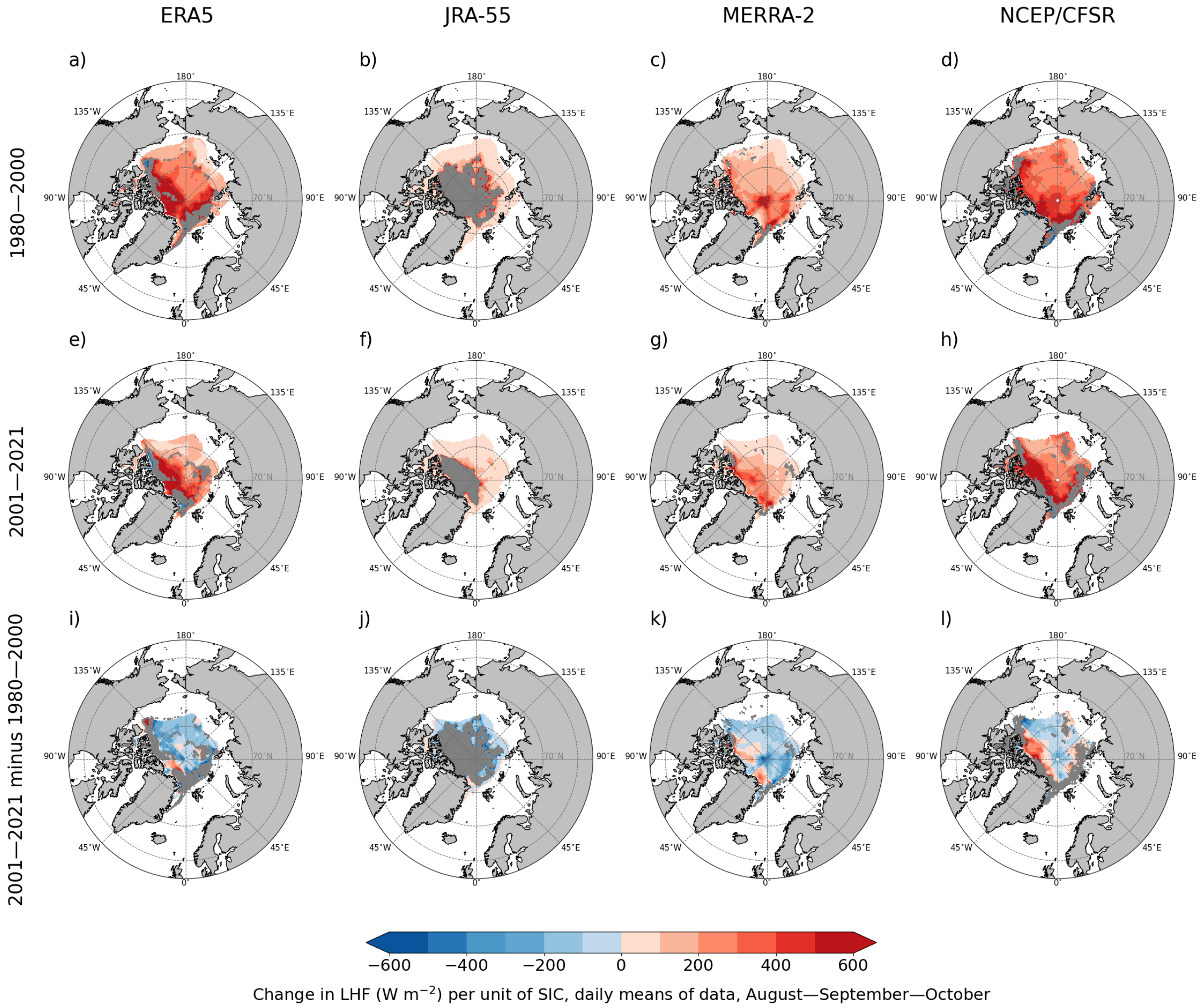

Figure S 6: Change in latent heat flux (W m^{-2}) per unit of change in sea-ice concentration (slope of regression line) in four reanalyses (columns), marine Arctic, August–September–October, based on the linear orthogonal-distance-regression (ODR) model. **a**–**d** depict the period 1980–2000, **e**–**h** period 2001–2021, and **i**–**l** show the 2001–2021 difference from 1980–2000. Dark grey indicates areas where the ODR model did not converge; in i–l, dark grey shows these areas in 1980–2000 and/or 2001–2021. Only grid cells with a mean of SIC > 0.5 were considered, and only statistically significant results within 95 % confidence interval are shown.

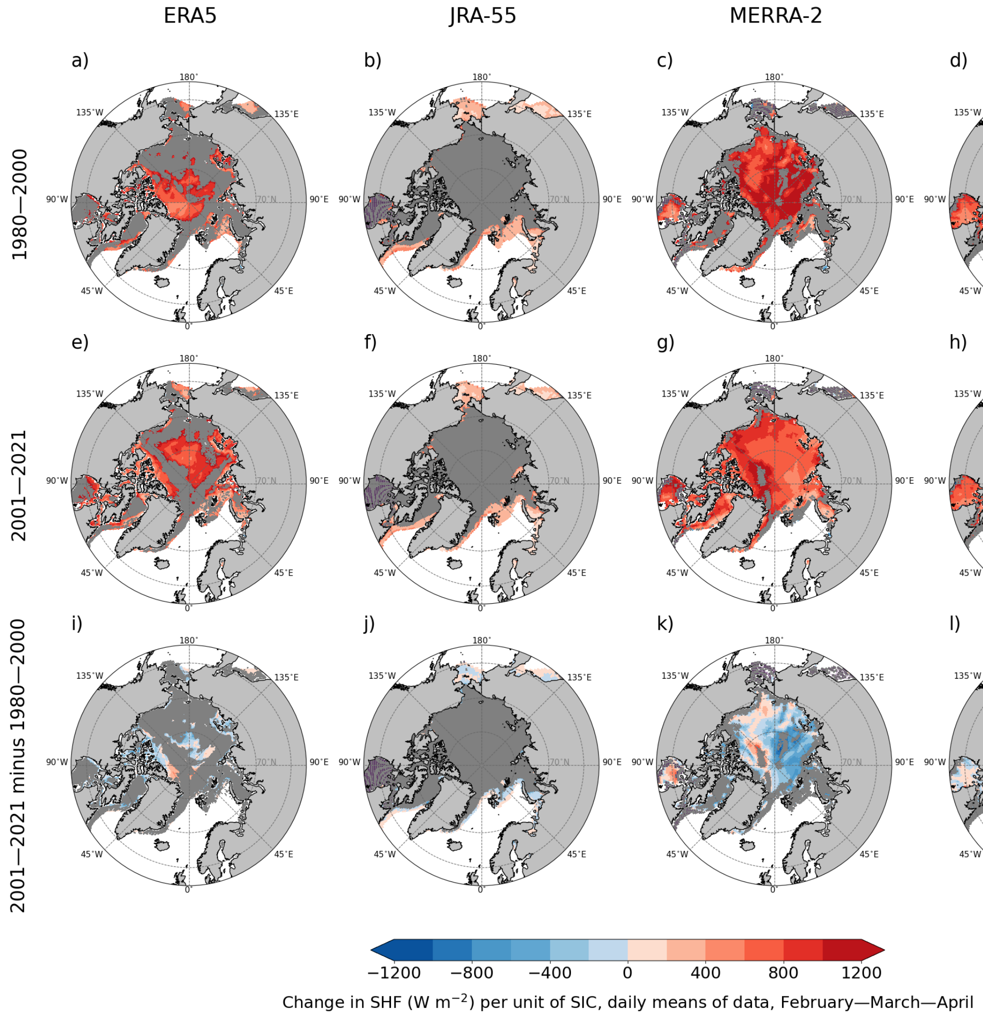

Figure S 7: Change in sensible heat flux (W m^{-2}) per unit of change in sea-ice concentration (slope of regression line) in four reanalyses (columns), marine Arctic, February–March–April, based on the linear orthogonal-distance-regression (ODR) model. **a**–**d** depict the period 1980–2000, **e**–**h** period 2001–2021, and **i**–**l** show the 2001–2021 difference from 1980–2000. Dark grey indicates areas where the ODR model did not converge; in i–l, dark grey shows these areas in 1980–2000 and/or 2001–2021. Only grid cells with a mean of SIC > 0.5 were considered, and only statistically significant results within 95 % confidence interval are shown.

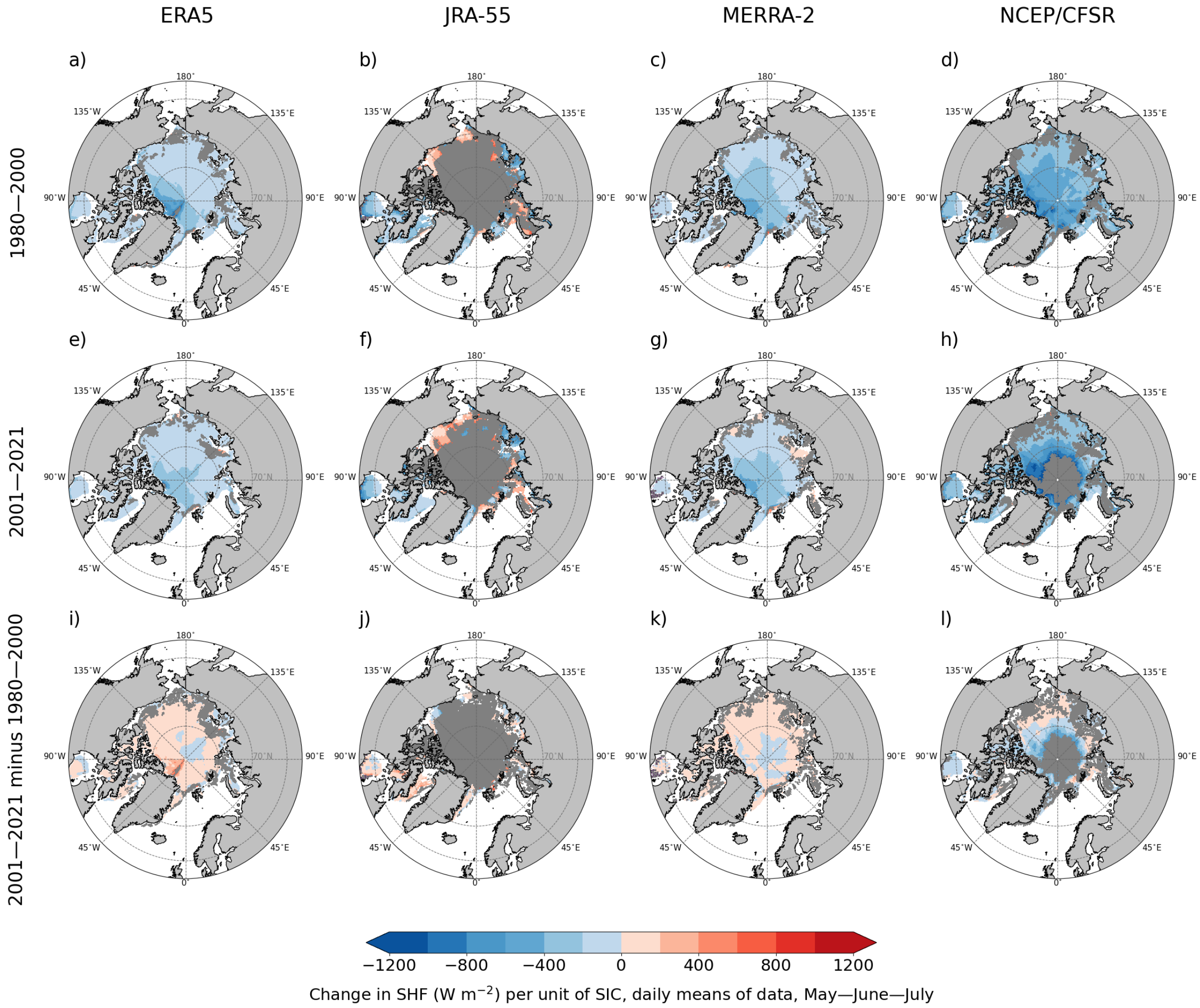

Figure S 8: Change in sensible heat flux (W m^{-2}) per unit of change in sea-ice concentration (slope of regression line) in four reanalyses (columns), marine Arctic, May–June–July, based on the linear orthogonal-distance-regression (ODR) model. **a–d** depict the period 1980–2000, **e–h** period 2001–2021, and **i–l** show the 2001–2021 difference from 1980–2000. Dark grey indicates areas where the ODR model did not converge; in i–l, dark grey shows these areas in 1980–2000 and/or 2001–2021. Only grid cells with a mean of SIC > 0.5 were considered, and only statistically significant results within 95 % confidence interval are shown.

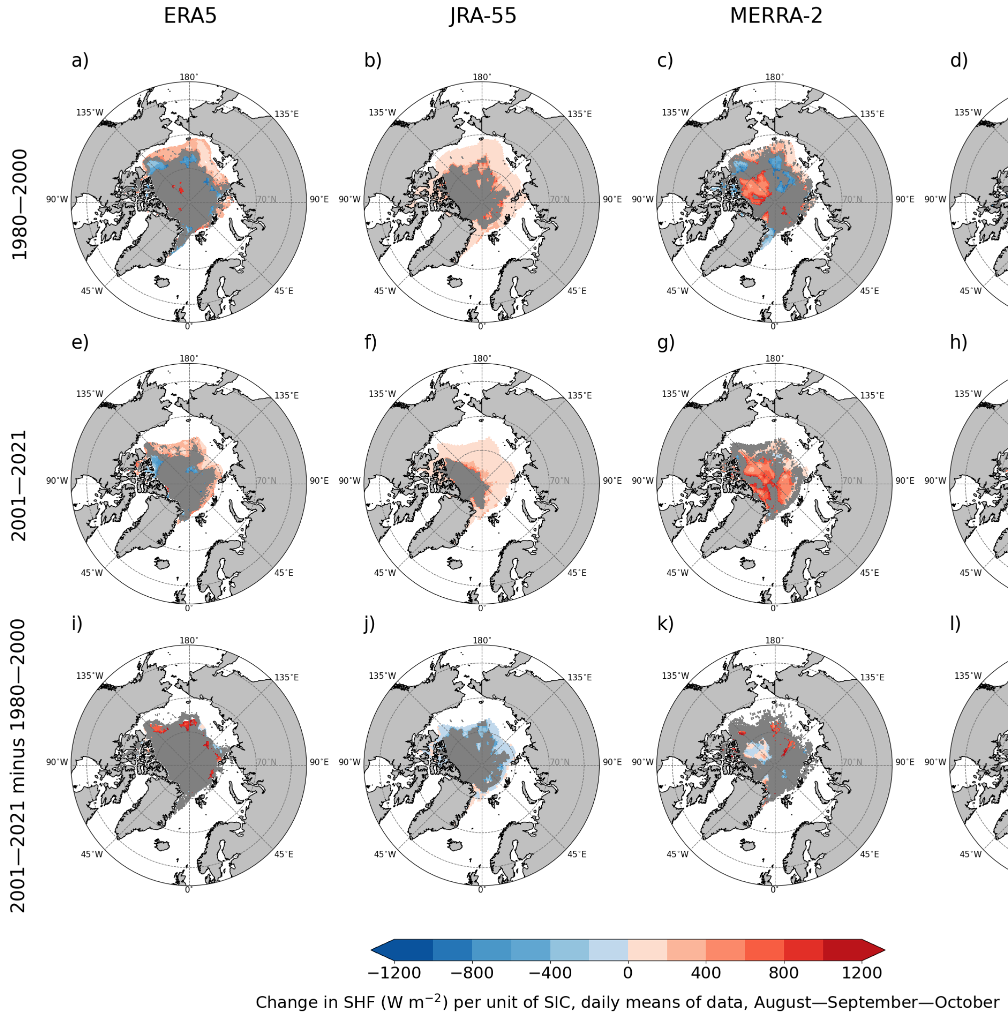

Figure S 9: Change in sensible heat flux (W m^{-2}) per unit of change in sea-ice concentration (slope of regression line) in four reanalyses (columns), marine Arctic, August–September–October, based on the linear orthogonal-distance-regression (ODR) model. **a**–**d** depict the period 1980–2000, **e**–**h** period 2001–2021, and **i**–**l** show the 2001–2021 difference from 1980–2000. Dark grey indicates areas where the ODR model did not converge; in i–l, dark grey shows these areas in 1980–2000 and/or 2001–2021. Only grid cells with a mean of SIC > 0.5 were considered, and only statistically significant results within 95 % confidence interval are shown.

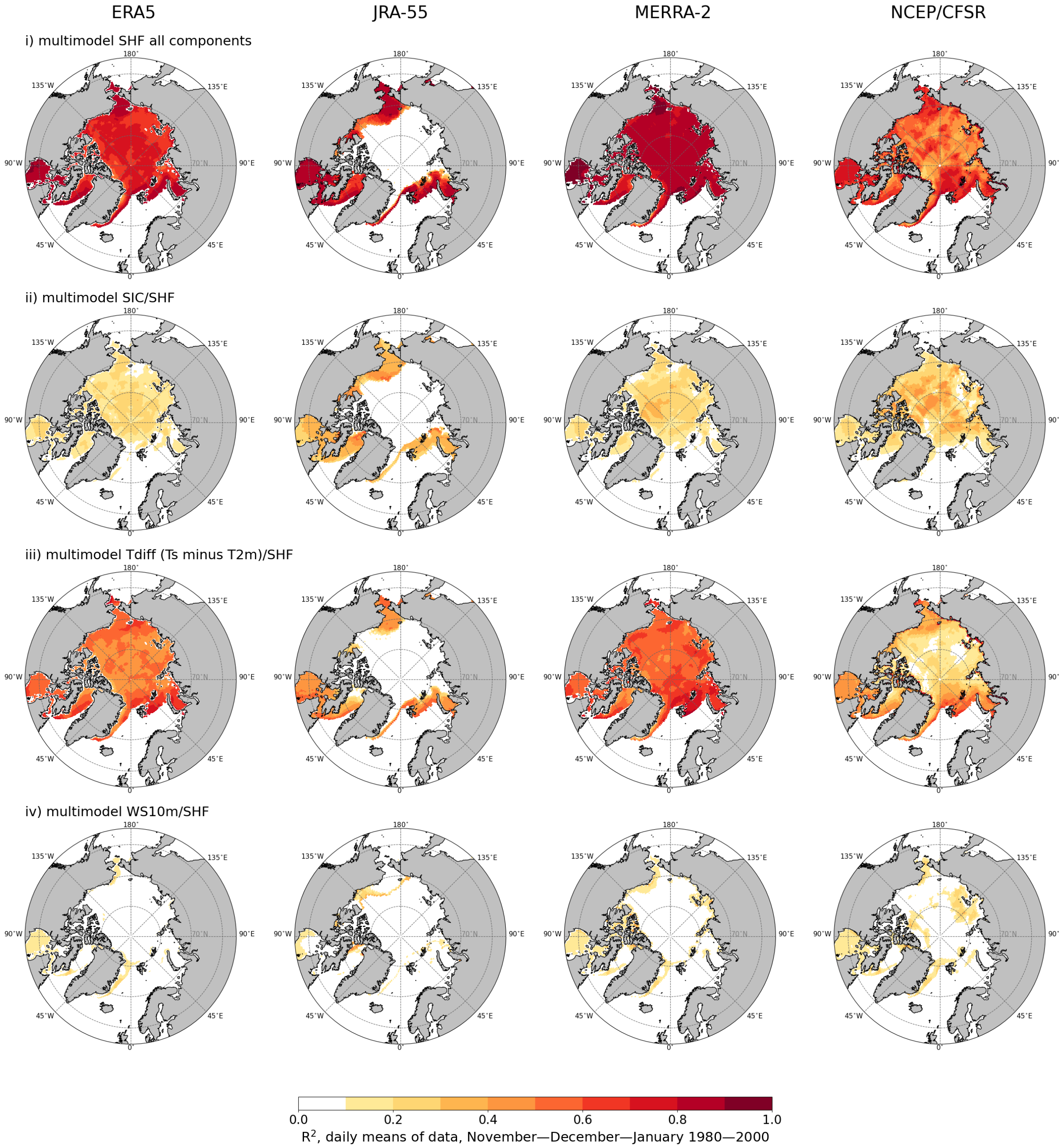

Figure S 10: Proportion of variance in the sensible heat flux (vSHF) explained by the linear ordinary-least-square regression model (coefficient of determination, R^2); daily means of data, November–December–January, 1980–2000. Row **i** - vSHF explained by all components: SIC/temperature difference (T_{2m} minus T_s, T_{diff})/wind speed (10 m, WS_{10m}); row **ii** - vSHF explained by the SIC/SHF component of the model; row **iii** - vSHF explained by the T_{diff}/SHF component of the model; row **iv** - vSHF explained by the WS_{10m}/SHF component of the model. Only grid cells with a mean of SIC $>$ 0.5 were considered.

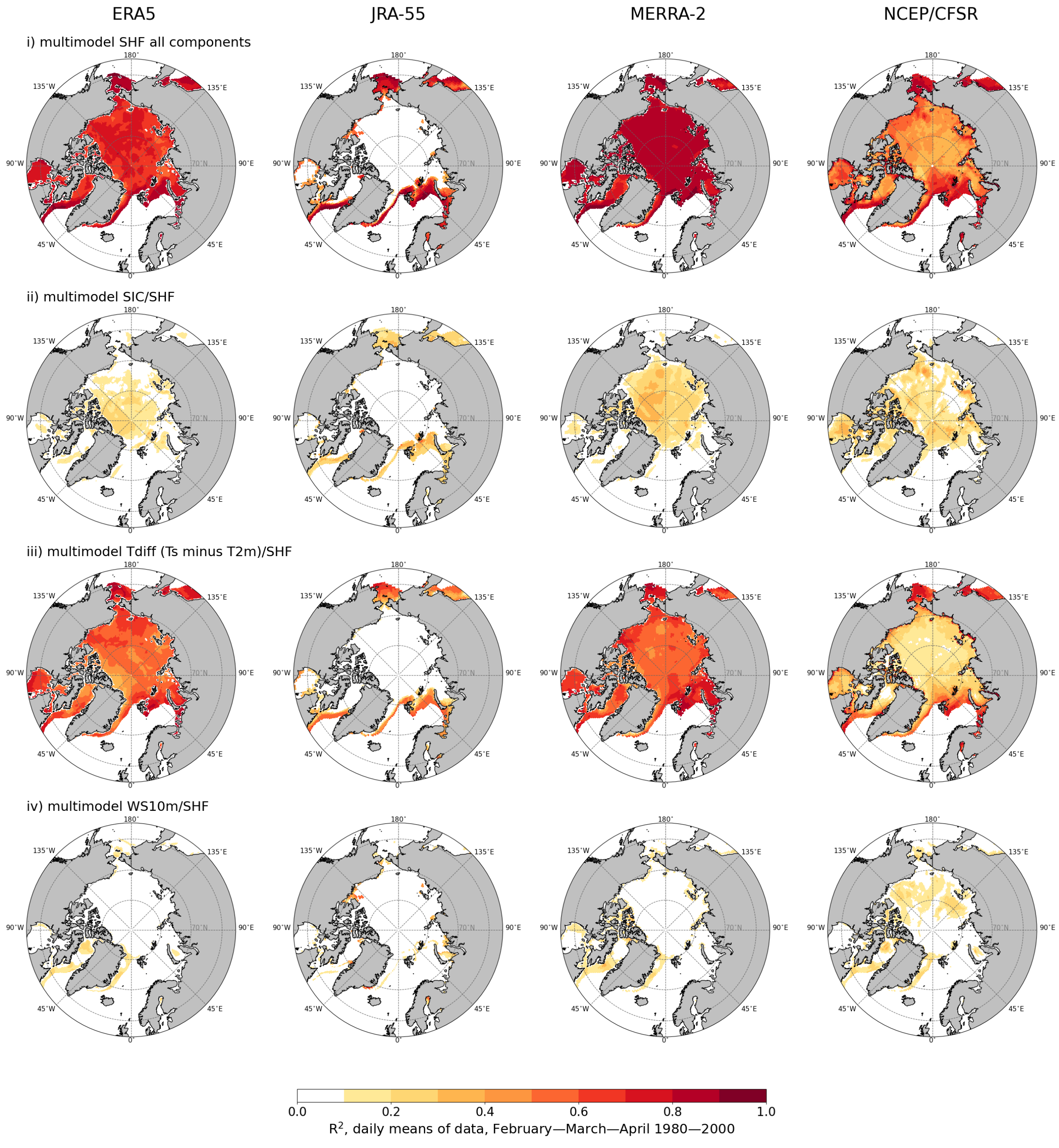

Figure S 11: Proportion of variance in the sensible heat flux (vSHF) explained by the linear ordinary-least-square regression model (coefficient of determination, R^2); daily means of data, February–March–April, 1980–2000. Row **i** - vSHF explained by all components: SIC/temperature difference (T_{2m} minus T_s, T_{diff})/wind speed (10 m, WS_{10m}); row **ii** - vSHF explained by the SIC/SHF component of the model; row **iii** - vSHF explained by the T_{diff}/SHF component of the model; row **iv** - vSHF explained by the WS_{10m}/SHF component of the model. Only grid cells with a mean of SIC > 0.5 were considered.

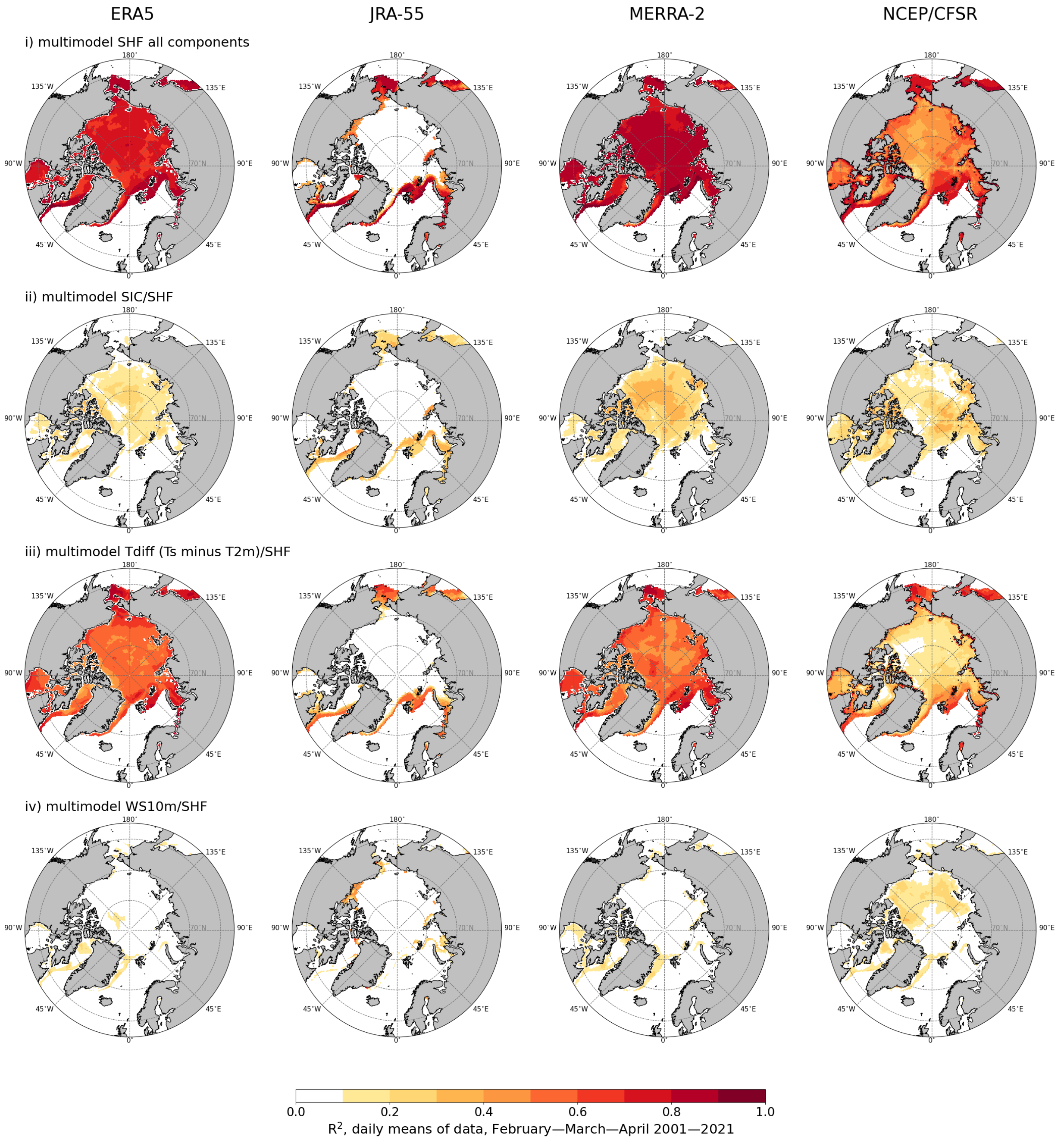

Figure S 12: Proportion of variance in the sensible heat flux (vSHF) explained by the linear ordinary-least-square regression model (coefficient of determination, R^2); daily means of data, February–March–April, 2001–2021. Row **i** - vSHF explained by all components: SIC/temperature difference (T_{2m} minus T_s, T_{diff})/wind speed (10 m, WS_{10m}); row **ii** - vSHF explained by the SIC/SHF component of the model; row **iii** - vSHF explained by the T_{diff}/SHF component of the model; row **iv** - vSHF explained by the WS_{10m}/SHF component of the model. Only grid cells with a mean of SIC $>$ 0.5 were considered.

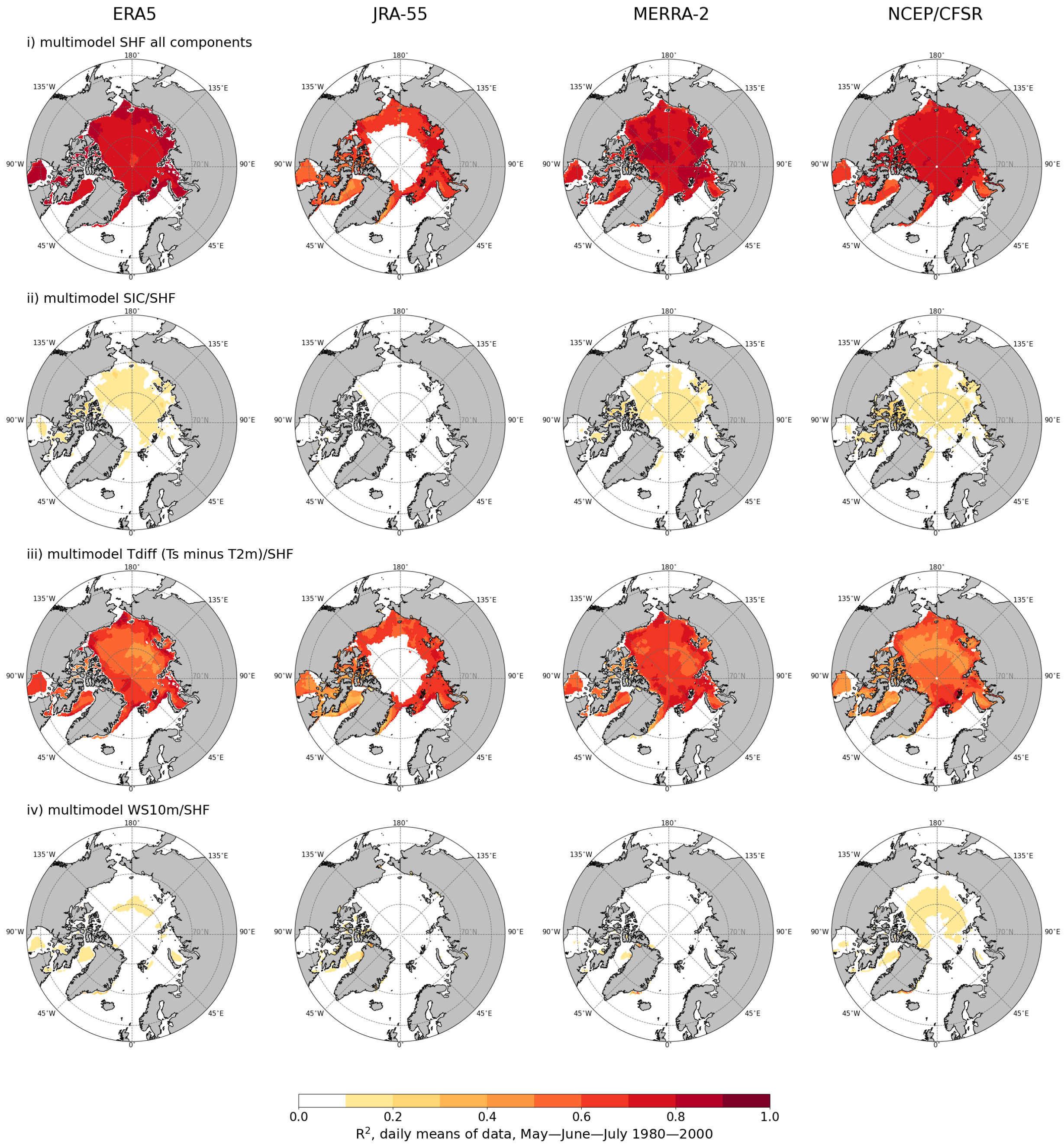

Figure S 13: Proportion of variance in the sensible heat flux (vSHF) explained by the linear ordinary-least-square regression model (coefficient of determination, R^2); daily means of data, May–June–July, 1980–2000. Row **i** - vSHF explained by all components: SIC/temperature difference (T_{2m} minus T_s, T_{diff})/wind speed (10 m, WS_{10m}); row **ii** - vSHF explained by the SIC/SHF component of the model; row **iii** - vSHF explained by the T_{diff}/SHF component of the model; row **iv** - vSHF explained by the WS_{10m}/SHF component of the model. Only grid cells with a mean of SIC $>$ 0.5 were considered.

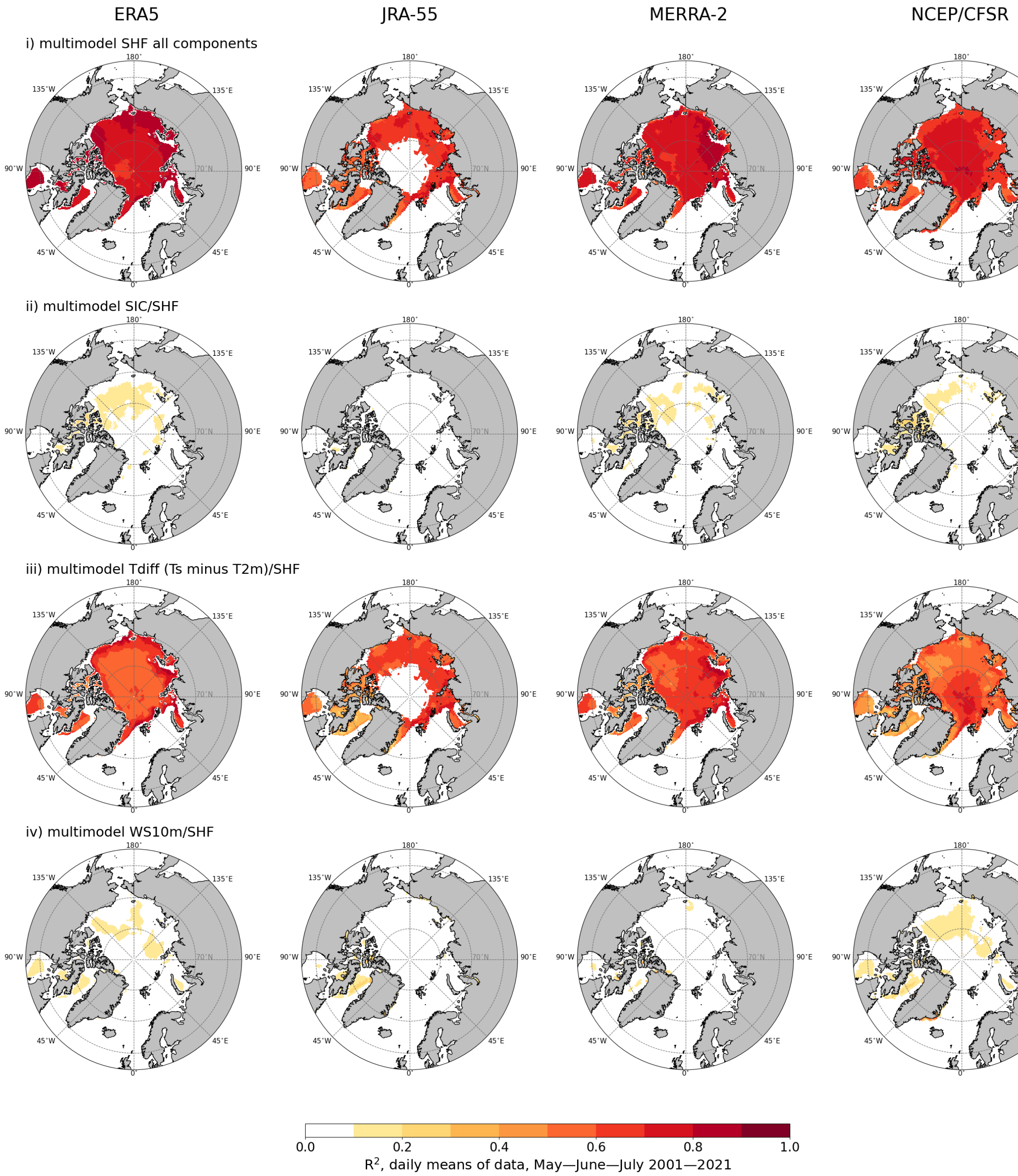

Figure S 14: Proportion of variance in the sensible heat flux (vSHF) explained by the linear ordinary-least-square regression model (coefficient of determination, R^2); daily means of data, May–June–July, 2001–2021. Row **i** - vSHF explained by all components: SIC/temperature difference (T_{2m} minus T_s, T_{diff})/wind speed (10 m, WS_{10m}); row **ii** - vSHF explained by the SIC/SHF component of the model; row **iii** - vSHF explained by the T_{diff}/SHF component of the model; row **iv** - vSHF explained by the WS_{10m}/SHF component of the model. Only grid cells with a mean of SIC > 0.5 were considered.

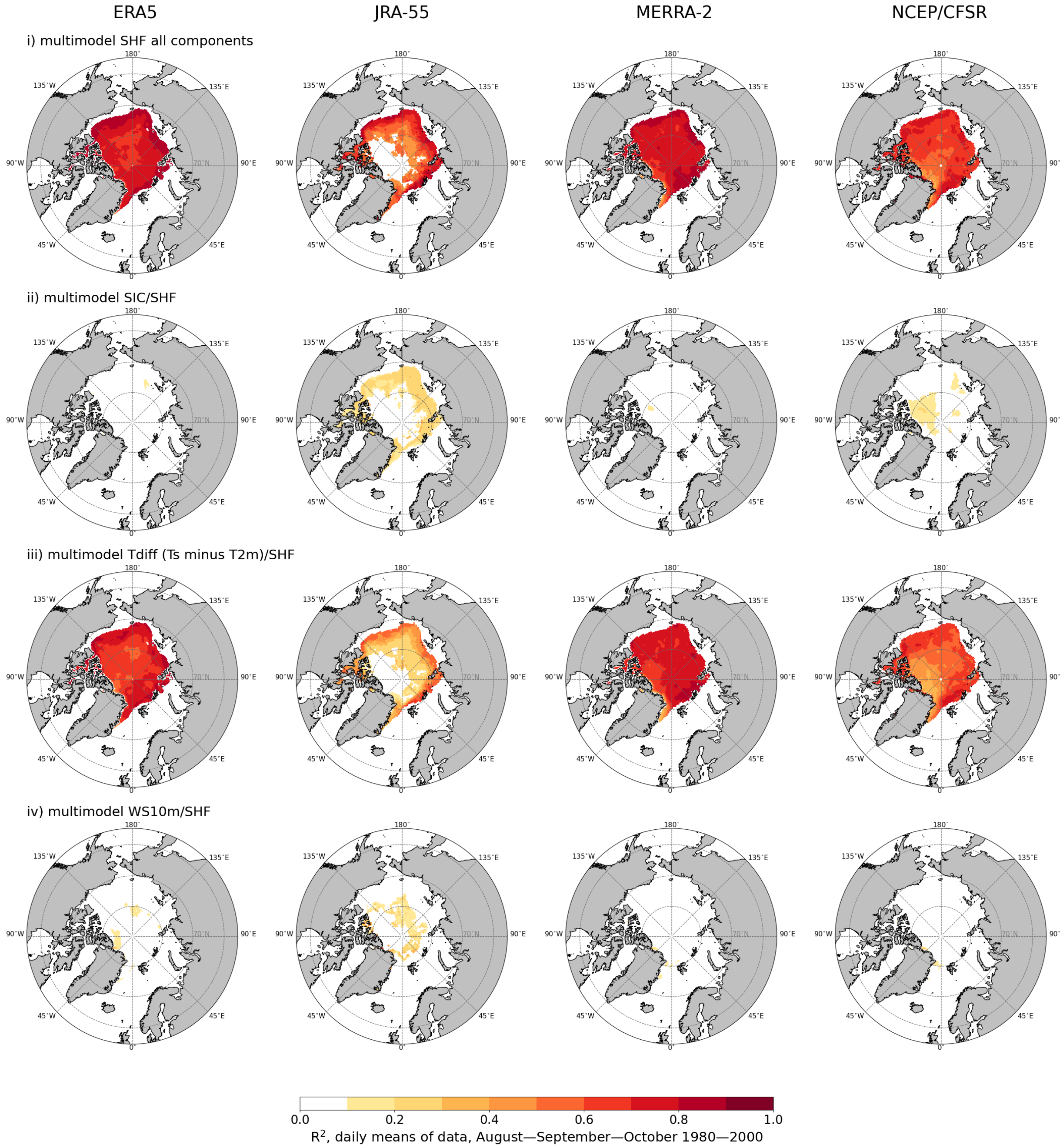

Figure S 15: Proportion of variance in the sensible heat flux (vSHF) explained by the linear ordinary-least-square regression model (coefficient of determination, R^2); daily means of data, August–September–October, 1980–2000. Row **i** - vSHF explained by all components: SIC/temperature difference (T_{2m} minus T_s, T_{diff})/wind speed (10 m, WS_{10m}); row **ii** - vSHF explained by the SIC/SHF component of the model; row **iii** - vSHF explained by the T_{diff}/SHF component of the model; row **iv** - vSHF explained by the WS_{10m}/SHF component of the model. Only grid cells with a mean of SIC > 0.5 were considered.

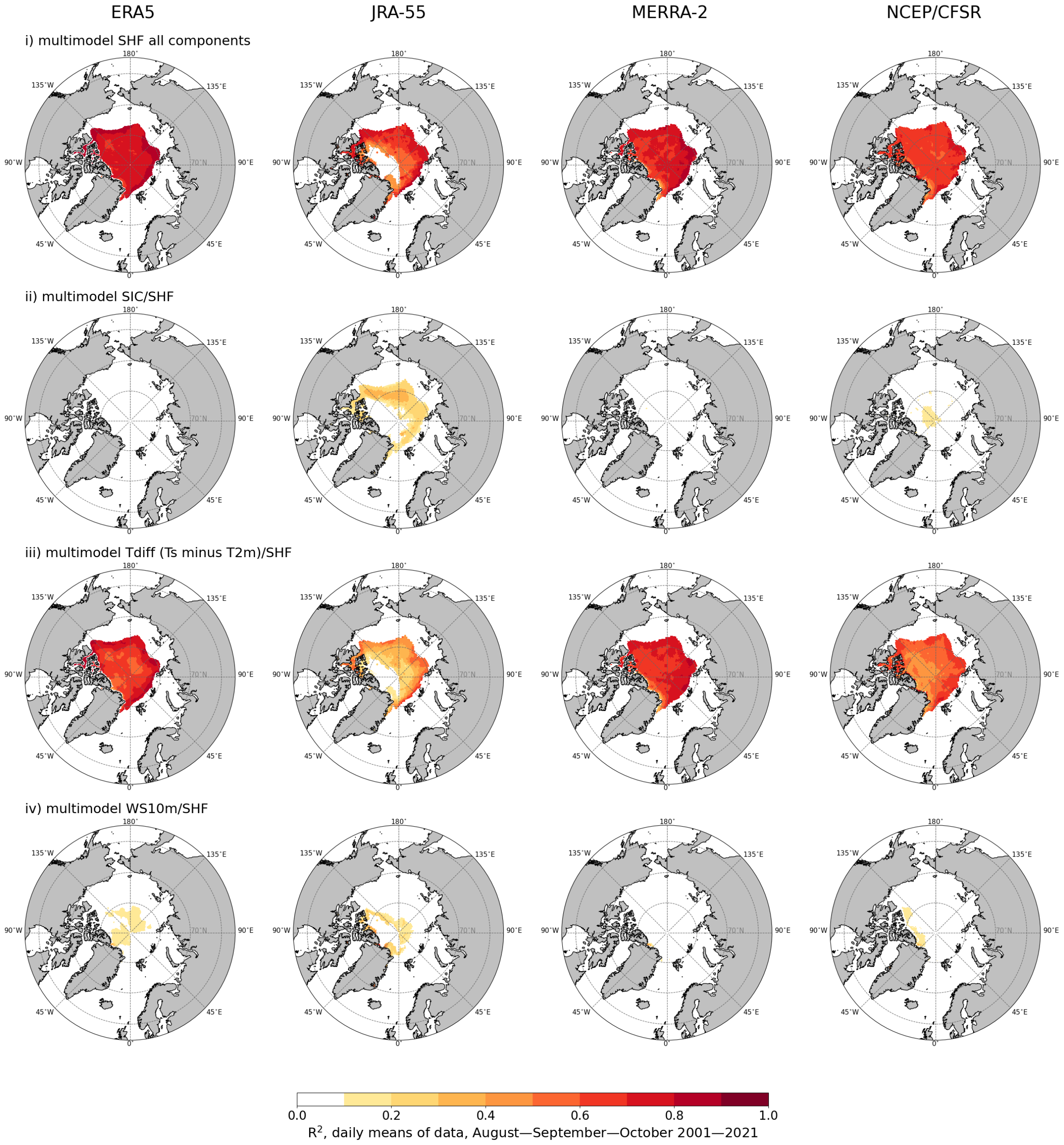

Figure S 16: Proportion of variance in the sensible heat flux (vSHF) explained by the linear ordinary-least-square regression model (coefficient of determination, R^2); daily means of data, August–September–October, 2001–2021. Row **i** - vSHF explained by all components: SIC/temperature difference (T_{2m} minus T_s, T_{diff})/wind speed (10 m, WS_{10m}); row **ii** - vSHF explained by the SIC/SHF component of the model; row **iii** - vSHF explained by the T_{diff}/SHF component of the model; row **iv** - vSHF explained by the WS_{10m}/SHF component of the model. Only grid cells with a mean of SIC > 0.5 were considered.

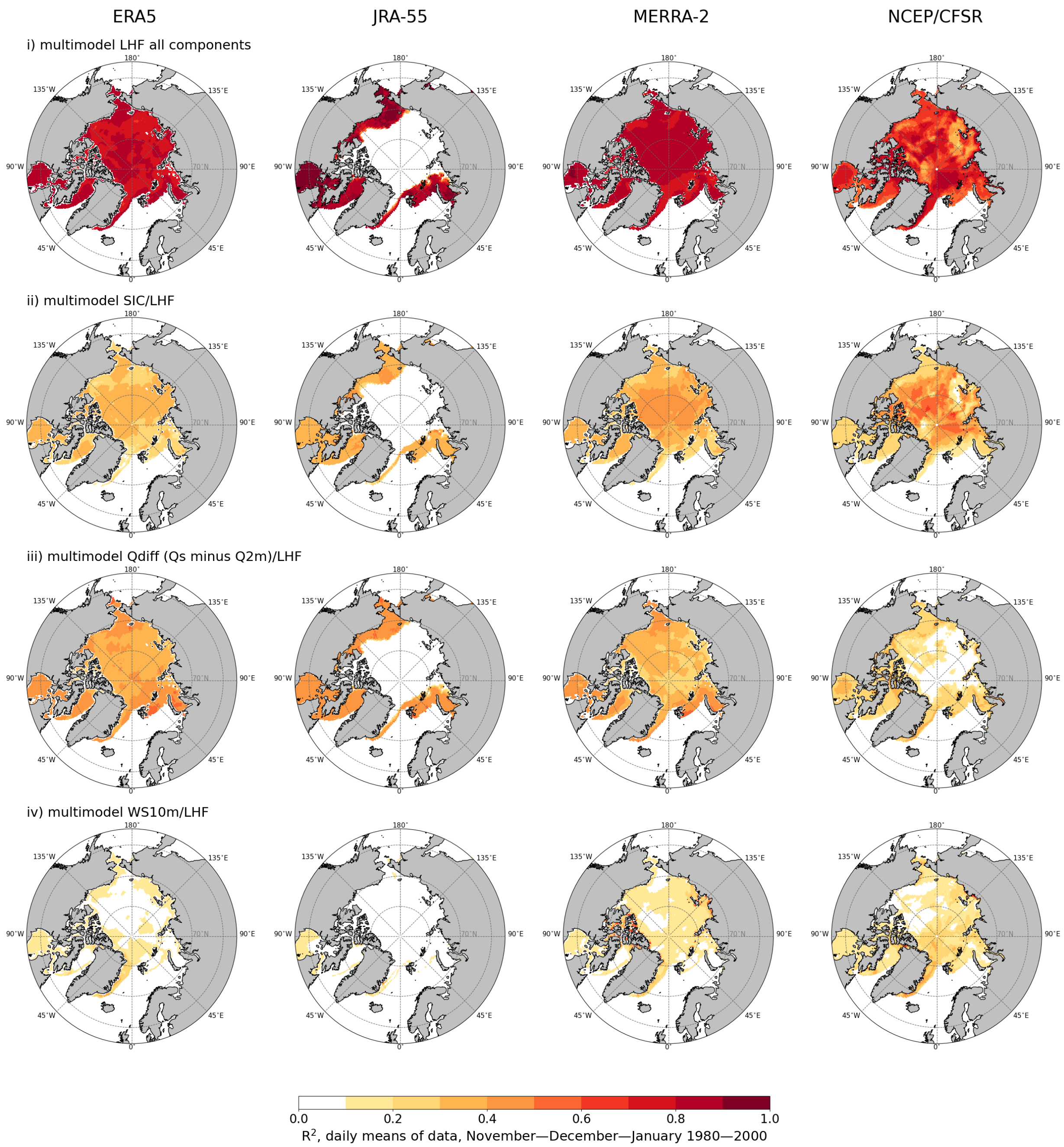

Figure S 17: Proportion of variance in the latent heat flux (vLHF) explained by the linear ordinary-least-square regression model (coefficient of determination, R^2); daily means of data, November–December–January, 1980–2000. Row **i** - vLHF explained by all components: SIC/specific-humidity difference (Q_{2m} minus Q_s, Q_{diff})/wind speed (10 m, WS_{10m}); row **ii** - vLHF explained by the SIC/LHF component of the model; row **iii** - vLHF explained by the Q_{diff}/LHF component of the model; row **iv** - vLHF explained by the WS_{10m}/LHF component of the model. Only grid cells with a mean of SIC > 0.5 were considered.

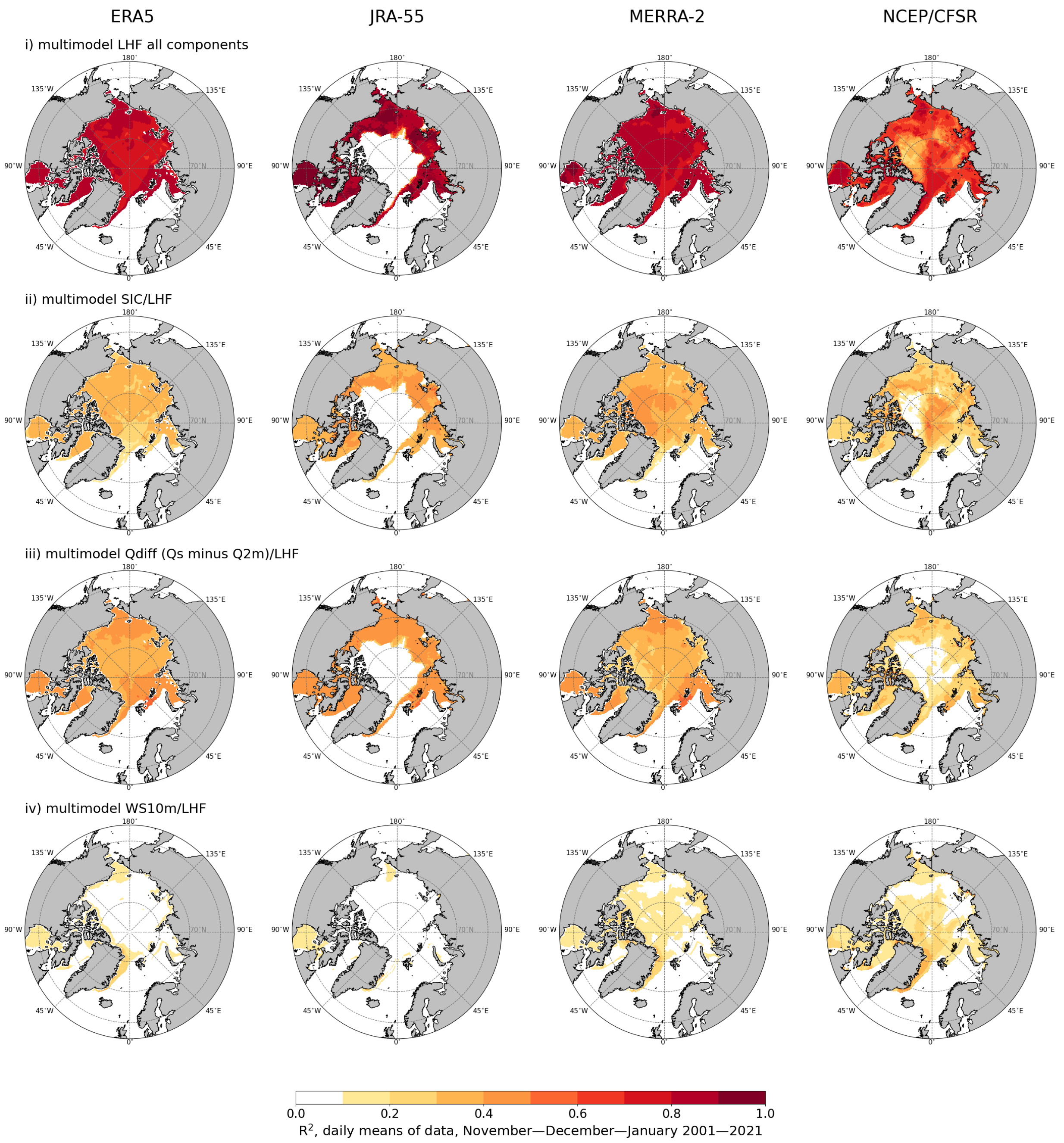

Figure S 18: Proportion of variance in the latent heat flux (vLHF) explained by the linear ordinary-least-square regression model (coefficient of determination, R^2); daily means of data, November–December–January, 2001–2021. Row **i** - vLHF explained by all components: SIC/specific-humidity difference (Q_{2m} minus Q_s, Q_{diff})/wind speed (10 m, WS_{10m}); row **ii** - vLHF explained by the SIC/LHF component of the model; row **iii** - vLHF explained by the Q_{diff}/LHF component of the model; row **iv** - vLHF explained by the WS_{10m}/LHF component of the model. Only grid cells with a mean of SIC > 0.5 were considered.

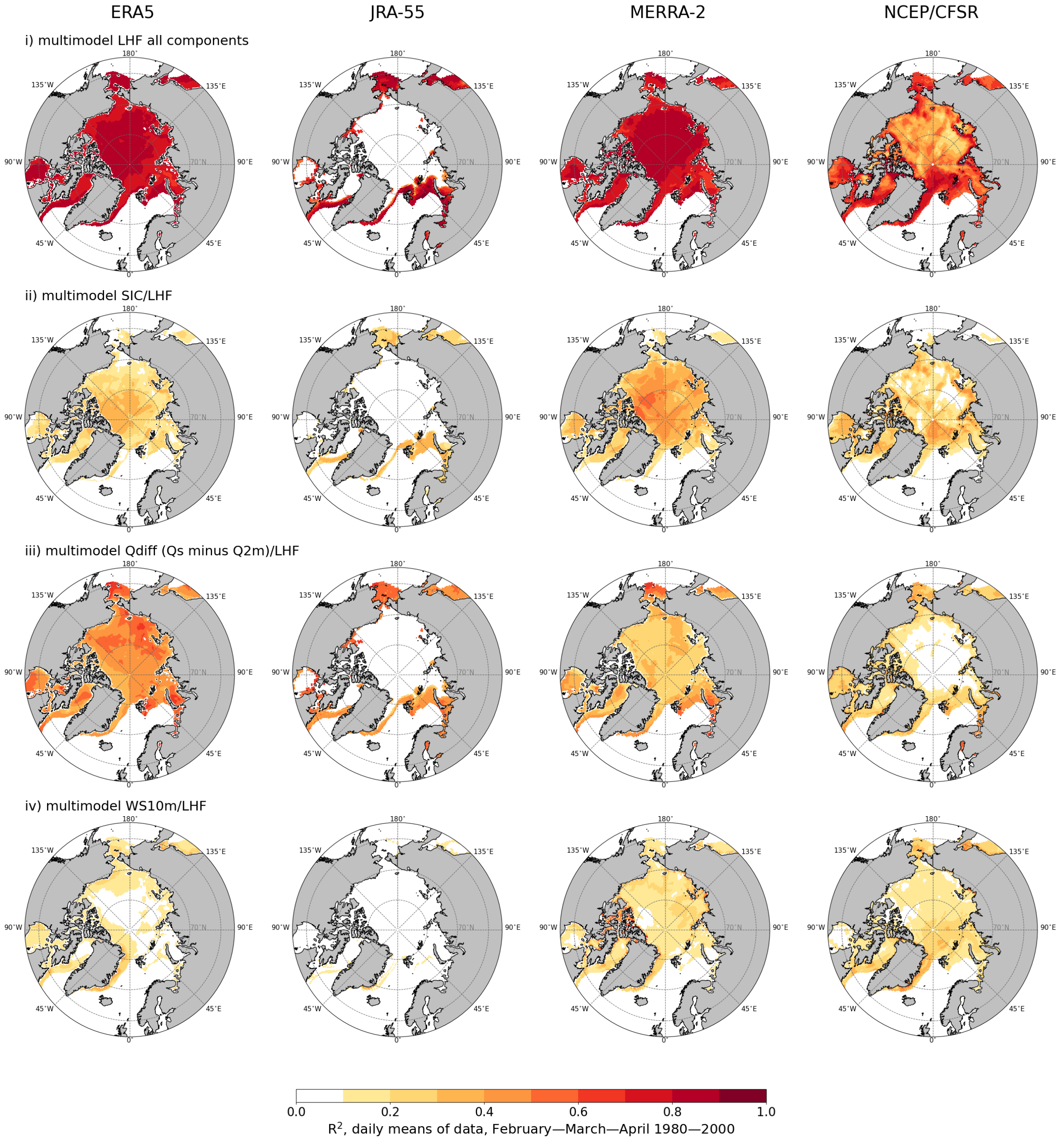

Figure S 19: Proportion of variance in the latent heat flux (vLHF) explained by the linear ordinary-least-square regression model (coefficient of determination, R^2); daily means of data, February–March–April, 1980–2000. Row **i** - vLHF explained by all components: SIC/specific-humidity difference (Q_{2m} minus Q_s, Q_{diff})/wind speed (10 m, WS_{10m}); row **ii** - vLHF explained by the SIC/LHF component of the model; row **iii** - vLHF explained by the Q_{diff}/LHF component of the model; row **iv** - vLHF explained by the WS_{10m}/LHF component of the model. Only grid cells with a mean of SIC > 0.5 were considered.

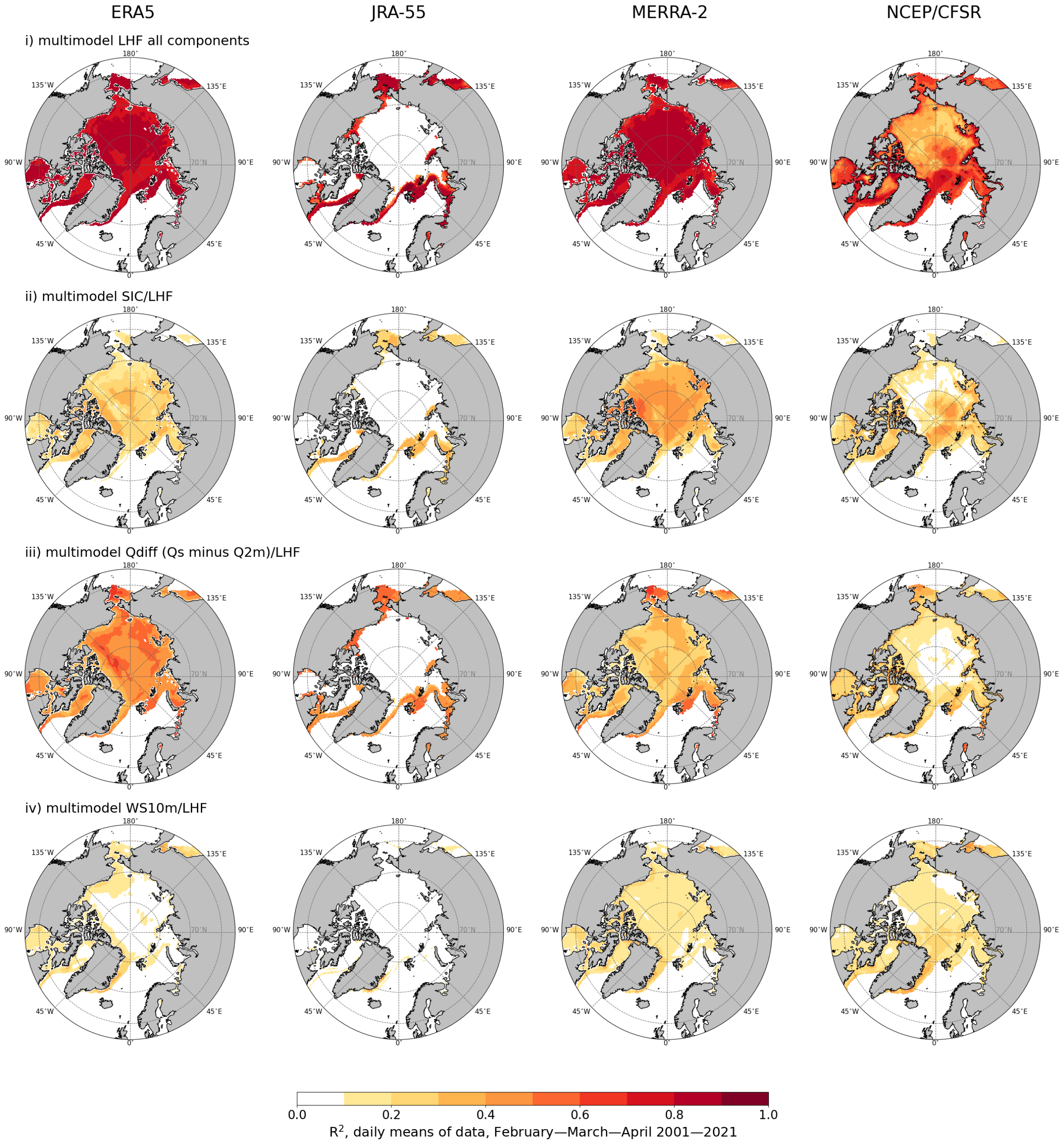

Figure S 20: Proportion of variance in the latent heat flux (vLHF) explained by the linear ordinary-least-square regression model (coefficient of determination, R^2); daily means of data, February–March–April, 2001–2021. Row **i** - vLHF explained by all components: SIC/specific-humidity difference (Q_{2m} minus Q_s, Q_{diff})/wind speed (10 m, WS_{10m}); row **ii** - vLHF explained by the SIC/LHF component of the model; row **iii** - vLHF explained by the Q_{diff}/LHF component of the model; row **iv** - vLHF explained by the WS_{10m}/LHF component of the model. Only grid cells with a mean of SIC > 0.5 were considered.

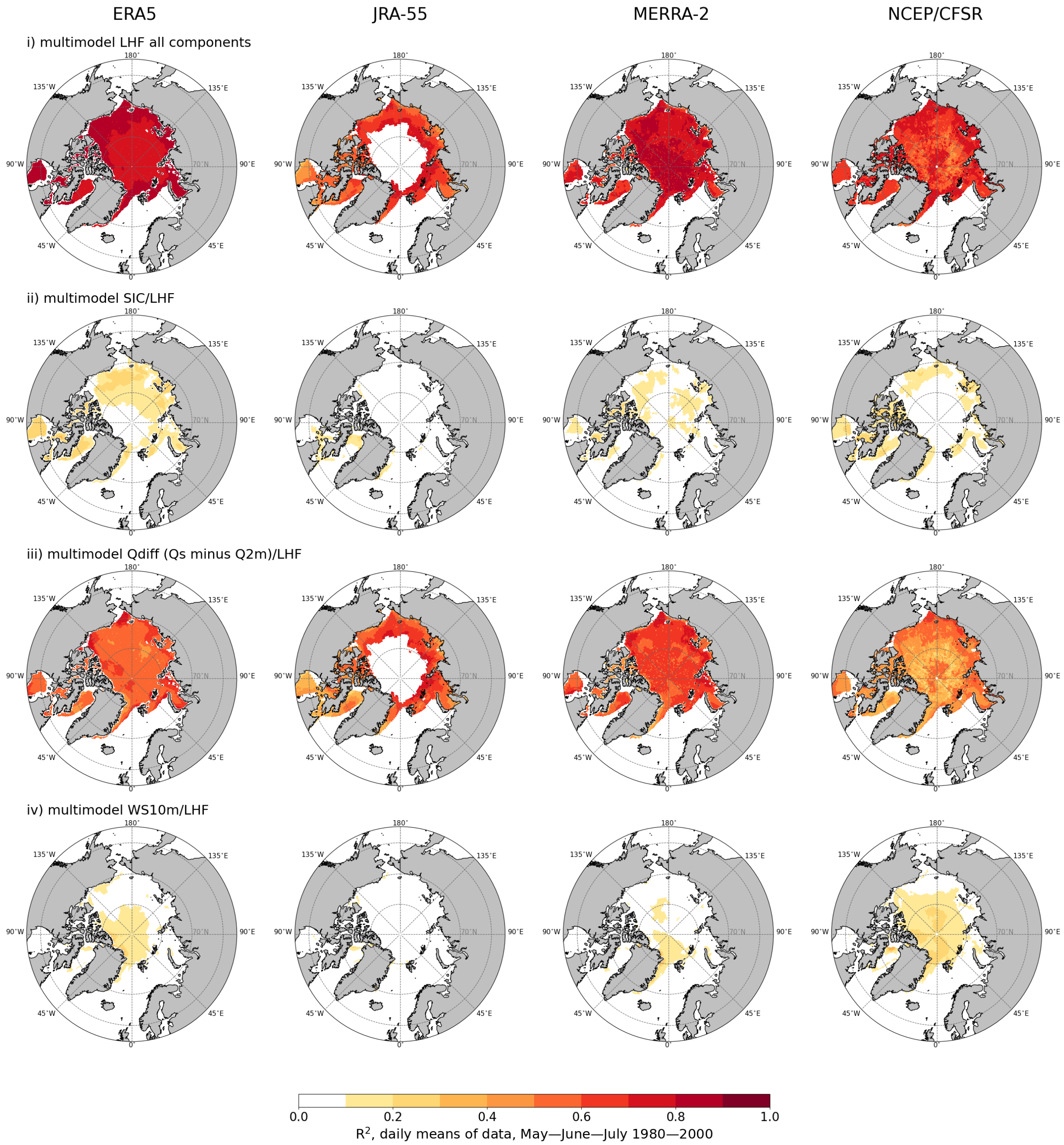

Figure S 21: Proportion of variance in the latent heat flux (vLHF) explained by the linear ordinary-least-square regression model (coefficient of determination, R^2); daily means of data, May–June–July, 1980–2000. Row **i** - vLHF explained by all components: SIC/specific-humidity difference (Q_{2m} minus Q_s, Q_{diff})/wind speed (10 m, WS_{10m}); row **ii** - vLHF explained by the SIC/LHF component of the model; row **iii** - vLHF explained by the Q_{diff}/LHF component of the model; row **iv** - vLHF explained by the WS_{10m}/LHF component of the model. Only grid cells with a mean of SIC > 0.5 were considered.

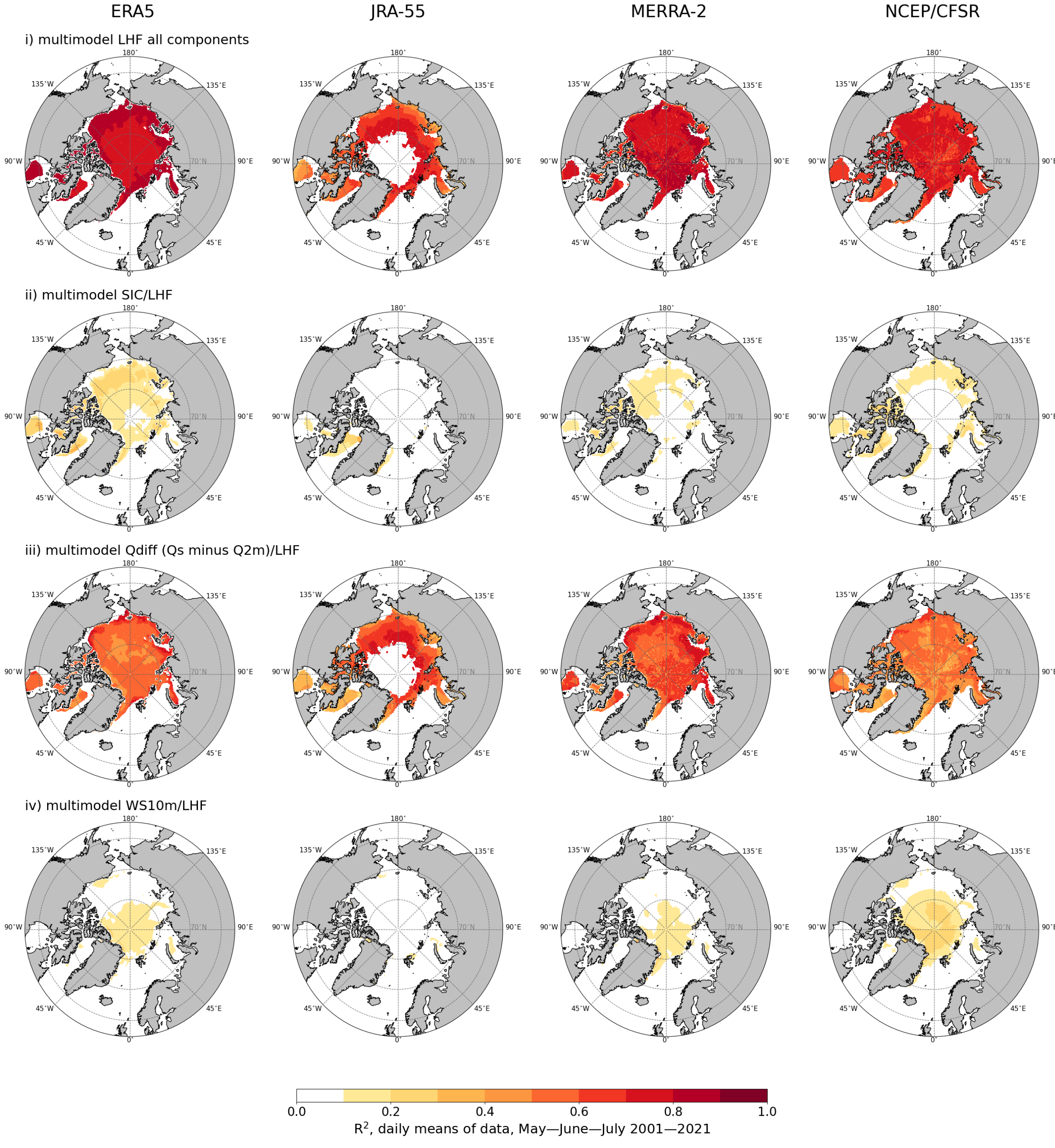

Figure S 22: Proportion of variance in the latent heat flux (vLHF) explained by the linear ordinary-least-square regression model (coefficient of determination, R^2); daily means of data, May–June–July, 2001–2021. Row **i** - vLHF explained by all components: SIC/specific-humidity difference (Q_{2m} minus Q_s, Q_{diff})/wind speed (10 m, WS_{10m}); row **ii** - vLHF explained by the SIC/LHF component of the model; row **iii** - vLHF explained by the Q_{diff}/LHF component of the model; row **iv** - vLHF explained by the WS_{10m}/LHF component of the model. Only grid cells with a mean of SIC > 0.5 were considered.

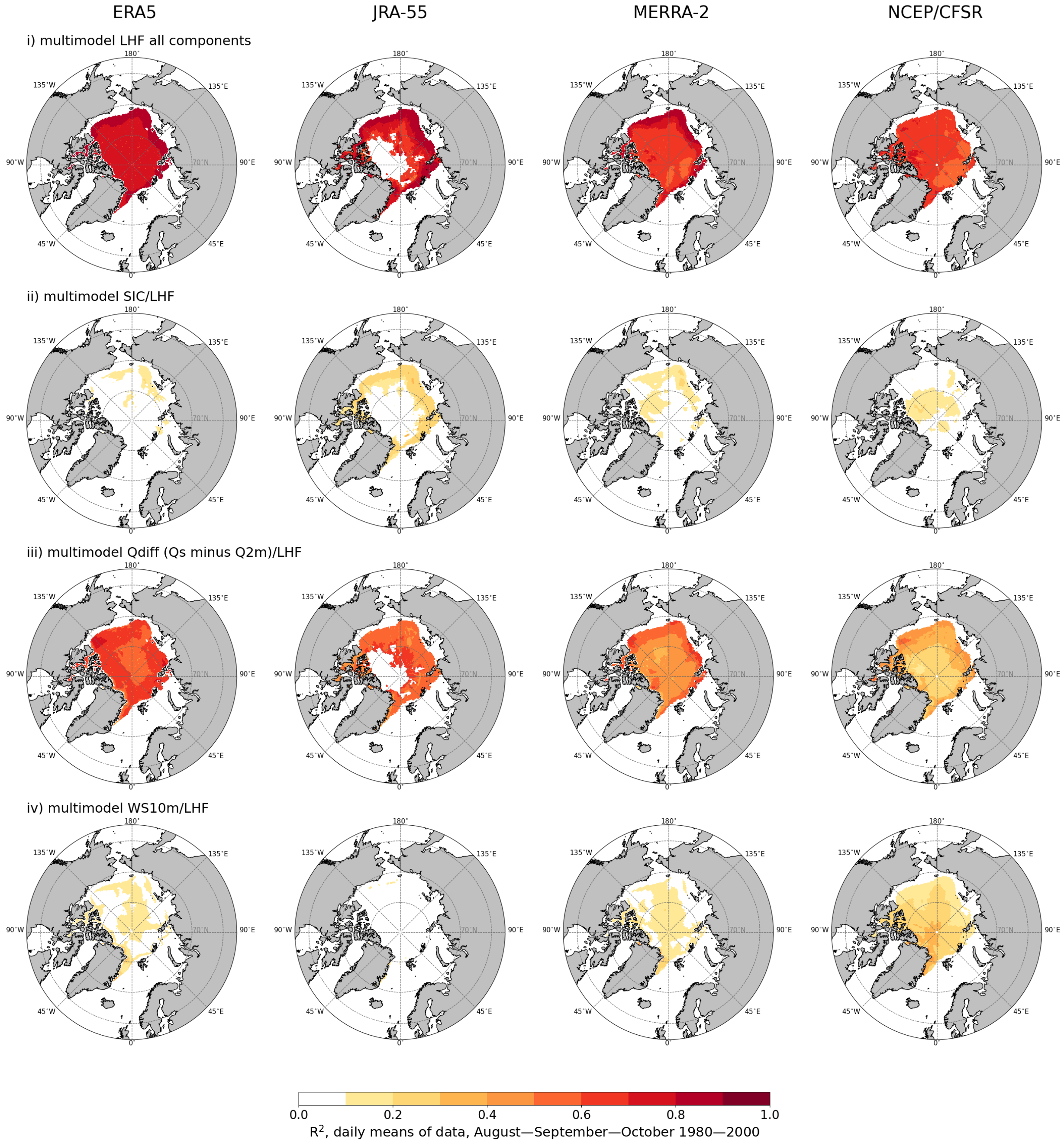

Figure S 23: Proportion of variance in the latent heat flux (vLHF) explained by the linear ordinary-least-square regression model (coefficient of determination, R^2); daily means of data, August–September–October, 1980–2000. Row **i** - vLHF explained by all components: SIC/specific-humidity difference (Q_{2m} minus Q_s, Q_{diff})/wind speed (10 m, WS_{10m}); row **ii** - vLHF explained by the SIC/LHF component of the model; row **iii** - vLHF explained by the Q_{diff}/LHF component of the model; row **iv** - vLHF explained by the WS_{10m}/LHF component of the model. Only grid cells with a mean of SIC > 0.5 were considered.

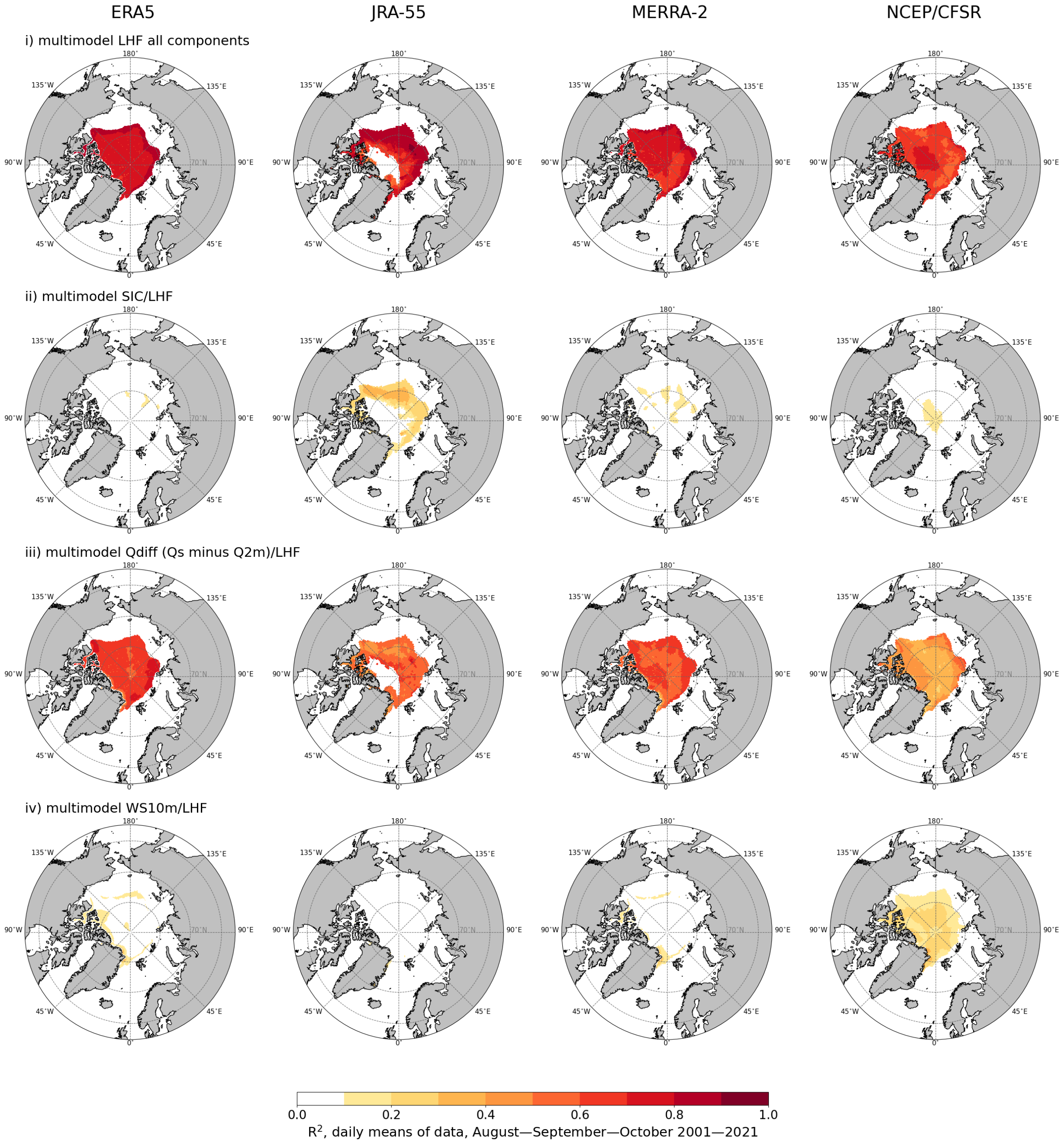

Figure S 24: Proportion of variance in the latent heat flux (vLHF) explained by the linear ordinary-least-square regression model (coefficient of determination, R^2); daily means of data, August–September–October, 2001–2021. Row **i** - vLHF explained by all components: SIC/specific-humidity difference (Q_{2m} minus Q_s, Q_{diff})/wind speed (10 m, WS_{10m}); row **ii** - vLHF explained by the SIC/LHF component of the model; row **iii** - vLHF explained by the Q_{diff}/LHF component of the model; row **iv** - vLHF explained by the WS_{10m}/LHF component of the model. Only grid cells with a mean of SIC > 0.5 were considered.